Structural characterisation of α-synuclein-membrane interactions and the resulting aggregation using small angle scattering - Supplementary materials

Céline Galvagnion,*,† Abigail Barclay,‡ Katarzyna Makasewicz,¶ Frederik Ravnkilde Marlet,† Martine Moulin,§ Juliette Devos,§ Sara Linse,¶ Anne Martel,§ Lionel Porcar,§ Emma Sparr,‖ Martin Cramer Pedersen,‡ Felix Roosen-Runge,⊥ Lise Arleth,‡ and Alexander K. Buell*,#

†*Department of Drug Design and Pharmacology, University of Copenhagen, 2100 Copenhagen, Denmark*

‡*Niels Bohr Institute, University of Copenhagen, 2100 Copenhagen, Denmark*

¶*Department of Biochemistry and Structural Biology, Lund University , SE22100 Lund, Sweden*

§*Institut Laue-Langevin, 71 avenue des Martyrs, 38042 Grenoble, France*

‖*Division of Physical Chemistry, Center for Chemistry and Chemical Engineering, Lund University, P.O. Box 124, SE-22100, Lund, Sweden*

⊥*Department of Biomedical Sciences and Biofilms Research Center for Biointerfaces, Malmö University, Malmö, Sweden*

#*Department of Biotechnology and Biomedicine, Technical University of Denmark, 2800 Kgs. Lyngby, Denmark*

E-mail: celine.galvagnion@sund.ku.dk; alebu@dtu.de

Supplementary Methods - Models for the analysis of the SAS data

Three-shell vesicle

The theoretical scattering form factor for polydisperse three-shell bilayer vesicles can be calculated as a spherical structure with a core representing the solvent surrounded by three shells. Polydispersity is taken into account by assuming a Gaussian distribution of sizes and fitting the sigma of the standard deviation of radii and thicknesses. The innermost and outermost shells have the relative scattering length density corresponding to the lipid hydrophilic headgroups, while the centre shell corresponds to the lipid hydrophobic tailgroups. The model is parameterised by i) the radius to the centre of the shell r, ii) the thickness of a single lipid, t, iii) the volume of a single lipid which is only allowed to vary within a few percent of the estimated nominal volume, ν_L, iv) the sigma of the standard deviation of radii, σ_{Radius}, v) the sigma of the standard deviation of lipid thickness, σ_t.

The inner and outer leaflets are assumed to have the same thickness, t. t is divided into t_{heads} and t_{tails} in proportion with their respective volumes. By dividing the volume of the vesicle by the volume of a single lipid, the average number of lipids per vesicle can be calculated and used to convert molar lipid concentrations into particle number densities, allowing to calculate the model on absolute scale.
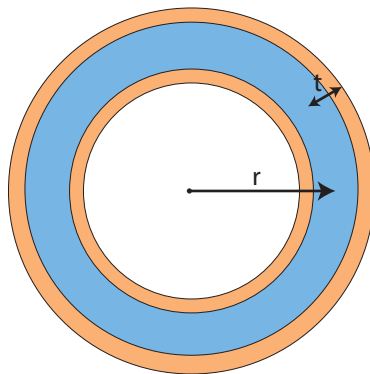
Figure S1: Schematic of the three-shell vesicle model where lipid headgroups are represented in orange and lipid tails are represented in blue. Not to scale.

Planar bilayer structure

The theoretical scattering form factor for lamellar phases[1,2] can be used to model "infinitely large" planar bilayer structures. The form factor of the local membrane structure can be seen at high-q, approximately above $q = 0.01$ Å^{-1}. The model can be implemented with either a uniform scattering length density or with distinct headgroup and tailgroup regions. The model is parameterised by i) the volume of a single lipid, V_L, ii) the thickness of a single lipid, t, iii) the sigma of the standard deviation of thicknesses, σ_t. The latter parameter needs to be included to accommodate polydispersity in lipid packing of the bilayer system, which contains vesicles but also other bilayer phases, such as lamelles.
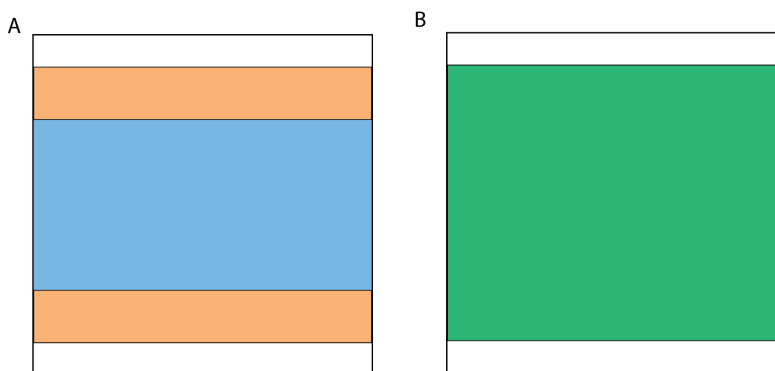

Figure S2: Schematic of the local planar bilayer model which focuses on the membrane structure. The absolute size of the particle cannot be resolved. A The orange and blue sections represent the lipid headgroups and tailgroups respectively. B Uniform contrast representing a simple plane.

Planar bilayer structure with Gaussian random coils

With this model, α-synuclein which is free in solution can additionally be accounted for alongside planar bilayer structures. The protein is described as Gaussian random coils. The model is calculated as

$$P(q) = P(q)_{\text{planar}} + n_{\text{protein}} \cdot P(q)_{\text{GRC}} \tag{1}$$

where $P(q)_{\text{planar}}$ is the form factor for lamella phases, n_{protein} is the particle number density of the protein and $P(q)_{\text{GRC}}$ is the Debye form factor.[3] The model has an additional parameter, iv) the radius of gyration of the Gaussian random coils, R_g.
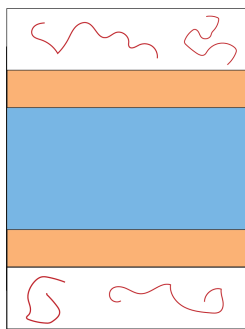

Figure S3: Schematic of the local planar bilayer model Gaussian random coils.

Discs decorated with Gaussian random coils

This model is akin to the model which has been used frequently to describe phospholipid nanodiscs [4,5] with a slight modification to account for the bound α-synuclein inspired by the SAXS model for α-synuclein-decorated vesicles presented by Cholak *et al.*[6] The geometric structure of the lipid bilayer is described as a collection of cylinders, representing the lipid headgroups and tails. The tail structure is surrounded by a hollow cylinder in this case representing a belt of α-synuclein. Polydispersity is taken into account by assuming a Gaussian distribution of radii. The model additionally accounts for scattering arising from α-synuclein embedded in the lipid bilayer by altering the scattering length densities assigned to each cylinder using Eqn 2. Gaussian random coils protrude from the outside and surface of

the disc using the same method derived by Pedersen and Gerstenberg [7,8] and used by Arleth *et al.* for their model of PEG-covered micelles .[9] Our reasoning leading to that structural model is that α-synuclein can both form the stabilising rim of lipid nanodiscs, i.e. act as a membrane scaffold protein (MSP),[10] as well as bind to the surfaces of discs stabilised by a MSP.[11] The model is parameterised by i) the radius of the disk, r, ii) the sigma of the standard deviation of radii, σ_r, iii) the thickness of a single lipid t, iv) the volume of a single lipid V_L, v) the volume of α-synuclein, $V_{\alpha\text{-syn}}$, vi) the width of the protein belt, w_{belt}, vii) the radius of gyration of the Gaussian random coils, $R_{g\,\alpha\text{-syn}}$, and viii) the molar ratio of lipid and bound protein, L/P. The average number of lipids per disc, N_L is calculated as V_{disc} / $(V_L + \text{L/P} * V_{\alpha\text{-syn:bilayer}})$ where V_{disc} is the volume of the disc excluding the protein belt and $V_{\alpha\text{-syn:bilayer}}$ is the volume of the fraction of α-synuclein embedded in the bilayer. The number of random coils per disc is $N_L/(\text{L/P})$. Furthermore N_L is then used to convert lipid concentration in molar to particle number density which can used to implement the model on absolute scale.
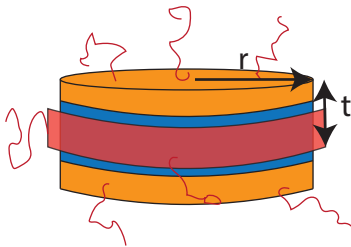

Figure S4: Schematic of the disc model with Gaussian random coils. The orange and blue shells represent lipid headgroups and tailgroups, respectively. The red hollow cylinder surrounding the tails represents a belt of α-synuclein and the red unfolded structures represent the protein extending from the surface of the disc. Not to scale.

The scattering length density for e.g. the outer discs representing lipid headgroups as well as some α-syn is calculated as:

$$\rho = \frac{(L/P \cdot b_{\text{heads}}) + (f_{\alpha\text{-syn, heads}} \cdot b_{\alpha\text{-syn}})}{(L/P \cdot V_{\text{heads}}) + (f_{\alpha\text{-syn, heads}} \cdot V_{\alpha\text{-syn}})} \tag{2}$$

where b are the scattering lengths, V are the molecular volumes and $f_{\alpha\text{-syn, heads}}$ is the

fraction of the α-synuclein monomer that is embedded in the lipid heads. Throughout this study, our modelling scheme has difficulties to accurately capture the dimensions of the protein. Therefore the radius of gyration $R_{g\,\alpha-syn}$ of the random coils was fixed to 18 Å, as calculated by Kohn's power law relationship for 44 amino acids,[12] the length of the C-terminal tail of α-synuclein that does not interact with the lipid bilayer.[13] Similarly we found the width of the protein belt, w_{belt}, did not have much influence on the shape of the model profile and was weakly constrained. Therefore w_{belt} was fixed to the diameter of an α-helix, 12Å, under the plausible assumption that α-synuclein forms a helical structure upon binding.[13]

Core-shell ribbon

This model calculates the form factor for a rectangular core-shell structure. The scattering length densities are again calculated according to Eqn 2. The outside shell has a thickness, i) t_{shell}, representing the lipid headgroups. The core represents the lipid tailgroups. The model has three free parameters describing the three lengths of the particle; ii) width, A, iii) height, B and iv) length, C. We also allow a Gaussian distribution of lengths in the width v) σ_A.
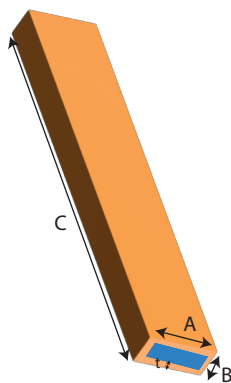

Figure S5: Schematic of the core-shell ribbon model where the orange shell represents the lipid headgroups mixed with some mount of α-synuclein and the blue core represents the lipid tailgroups mixed with some α-synuclein.

Core-shell cylinder decorated with Gaussian random coils

This model follows the same philosophy as our 'Disc with Gaussian ranom coils' model, with a smaller inner cylinder representing the lipid tailgroups and a larger outer cylinder representing the lipid headgroups. Gaussian random coils decorate the lengths of the cylinder. The free parameters of the model are therefore i) the length of the cylinder, L, ii) the radius of the inner cylinder, R, iii) the thickness of the shell, t_{shell}, iv) the radius of gyration of the protruding Gaussian random coils, R_g, and v) the molar ratio of lipids and bound protein L/P.
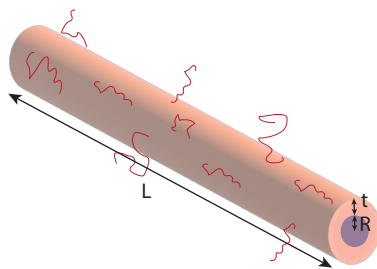

Figure S6: Schematic of the core-shell cylinder with Gaussian random coils. The orange shell represents the lipid headgroups mixed with some mount of α-synuclein and the blue core represents the lipid tailgroups mixed with some α-synuclein. The red represent the protein extending from the surface of the structure.

Modelling of stopped-flow SAXS data of DLPS and DMPS interaction with α-synuclein

The stopped-flow SAXS data (Figure 2) could not be converted to absolute scale, presumably due to some problems with background subtraction, and so a free scale parameter had to be employed during the model refinement. For consistency, we only fit the scale for the first DLPS and DMPS SAXS profiles and kept the scale fixed in subsequent refinements (Tables 3 and 4). Furthermore we observed that the molecular volumes for DLPS and DMPS did not need to be adjusted from their pre-estimated values and hence they were kept fixed throughout the data series to avoid overfitting.

Modelling of SAXS data of DLPS and DMPS interaction with α-synuclein and treated with proteinase K

In Figure 1, our fits of the SAXS data of DLPS vesicles are shown. The lipid volume V_{lipid} stays close to the starting value previously determined in the literature (912 Å^3 [14]). The area per lipid headgroup (A_{head}) can be deduced from the model fit results as V_{lipid} / t_{lipid} with the thickness of one lipid leaflet t_{lipid} and lies around 55 Å^2, which is in close agreement with the reports by Szekely *et al.* who found A_{head} to be 60.5 Å^2 for DLPS in the fluid phase. [15] The obtained mean radius of the DLPS vesicles of 210 Å is reasonable with respect to the extrusion preparation, and shows a small polydispersity, characterized via a relative standard deviation σ_{Radius} of 10%.

In order to achieve a satisfying fit, the DLPS vesicles formed after PK treatment of the mixtures require a polydisperse distribution of thicknesses of the lipid shell as well as the radius, whereas the initial intact vesicles only required a distribution of radii. This is likely due to the interaction of the heterogeneous mixture of the short peptides that result from the proteolytic digestion of the α-synuclein with the lipid bilayer. For the PK treated α-synuclein:DMPS mixtures, the $p(r)$-distribution profile has a similar shape to the one from pure DMPS, but the particles do not appear to revert to their original maximum dimensions (Figure 1 B : green). The structural parameters of the bilayer, on the other hand, are close to those before protein addition (Table 1 and 5). The thickness of the bilayer is identical but appears more polydisperse, as manifested by the more smeared out intensity maximum corresponding to the bilayer thickness. The molecular volume per lipid appears very slightly lower which could suggest some minor residual disturbance in the lipid packing.

For both the DLPS- and DMPS-α-synuclein mixtures, we refine populations of polydisperse discs with mean radii of around 140 Å. The thickness of the bilayer was found to be identical within error to the dimensions refined from the pure lipid data in Table 1. The refined molecular volumes for both DLPS and DMPS are 90% of those found in Table 1 which could potentially be explained by the difference in packing of lipids in vesicles and

discs. The refined volume for α-synuclein is 21300 Å^3 in both cases, which is 20% larger than the volume estimated using the average mass density of proteins as 1.35 cm^2 g^{-1}[16] (Table S1).

The SAXS profiles of DMPS model membranes in the presence of PK-pre-digested α-synuclein is characterized by an increased underlying intensity at mid- and high-q. The position of the minimum and bump (at $q \sim 0.04$ to 0.1 Å^{-1}) is unchanged compared with the data of pure DMPS (Figure S9: purple and red). This observation is consistent with conserved lipid structures with α-synuclein in a disordered conformation both in solution and decorating the lipids. From the $p(r)$-distributions it is evident that the overall planar structure is hardly affected by this short peptide-membrane interaction.

Modelling of temperature dependent SAXS data of DLPS and DMPS interaction with α-synuclein

The scattering profiles of the first five temperatures in Figure 3 (14 °C to 18 °C) of the α-synuclein:DMPS mixture lie approximately on top of each other. The corresponding $p(r)$-distribution profiles indicate very large particles with a D_{max} of at least 600 Å but which are not characteristic of any homogeneous, well-defined lipid vesicle population. Rather the $p(r)$-distribution suggests large planar or nearly planar structures[17]. Between 19 °C and 20 °C, however, a clear transition can be observed, corresponding to the melting of α-synuclein bound DMPS bilayers. The temperature-dependence of the profiles levels off again around 25°C suggesting the DMPS:α-synuclein co-structures may have reached a new (meta-)stable structural state. At these temperatures (T above 25°C), the $p(r)$-distribution profiles resemble that of disk-like particles[18][?] with a prominent flat maximum at $r = 50$ to 150 Å and a tail at long distances (Figure 3A). The disc-like particles appear much smaller than the initial aggregates. We attempted to refine structural models against data collected at various temperatures (Figure 3C). At 14 °C, the low-q data is again not compatible with a vesicle model. We therefore focus our modeling on the range $q = 0.02$ Å^{-1} and

upwards, in order to investigate properties of the bilayer rather than the whole structure. We again use the planar bilayer model, but with an altered scattering length density to reflect the previously determined stoichiometry at this temperature (i.e. 300 DMPS lipids per α-synuclein monomer).[19] Additionally, we use the form factor for Gaussian random coils to model the remaining free α-synuclein which have a non-negligible contribution to the scattering intensity. We find our description of the bilayer to be in line with the data (Table 6), refining a molecular volume for DMPS of 987 Å^3 which is in close agreement the pre-estimated value of 978 Å^3 ,[20] as well as observing an increase in the thickness of the lipid leaflets compared to DMPS lipid structures without α-synuclein. The refined R_g of the unbound α-synuclein of 31 Å is in close agreement with Kohn's estimation of 37 Å for 140 residues,[12] and with our SANS data from d-α-synuclein alone (Figure S12). We find that the initial state of DMPS is fully restored upon cooling-induced dissociation of α-synuclein, despite the fact that the initial state appears to be a heterogeneous mixed lipid phase rather than a well-defined single species. For temperatures above 21°C, i.e. just above the transition, the low-q slope of X-ray scattering profiles of DMPS:α-synuclein mixtures becomes more gentle and the 'Disc with Gaussian random coils' model, introduced above and described in the SI, can be employed. We fix the volume of DMPS to 987 Å^3 in line with the results reported in Table 6. At 21 °C, the model achieves an excellent fit (Figure 3C, Table 7). A ratio of lipid to bound-α-synuclein of 36 ± 7 is found, corresponding to around 90% of α-synuclein being bound which is possibly overestimated for 21 °C. At 30 °C the fit is satisfactory, although it overshoots the minimum at q=0.1, possibly suggesting the model is too simple to explain the DMPS:α-synuclein mixtures in this high binding regime. At 30 °C we assume that $\sim$100% of α-synuclein is bound to the lipid bilayer and therefore the molar ratio is fixed to 30:1 in line with the experimental concentrations. The model fit results show polydisperse discs with an average radius and bilayer thickness of 170 Å and 50 Å, respectively at 21 °C, which are reduced to 142 Å and 38 Å at 30 °C (Table 7).

Modelling lipid elongation during amyloid formation

The SANS data in 100% D_2O presented in Figure 5, were modelled with cylinders assigned a "bulk" scattering length density corresponding to that of pure DLPS. A free scale parameter was required to correct the scattering length density of the lipid particle as more d-α-synuclein becomes incorporated and decreases the overall contrast, as well as ambiguity in calculating the number density of scatterers.

Model implementation

All of the form factors used are available in the literature .[21] The models were implemented in $WillItFit$.[22] The models are implemented on absolute scale by exploiting the experimental lipid concentrations, as well as calculating scattering lengths of each model component through its corresponding molecular composition, as listed in Table S1. Molecular volumes are forced to remain within ten percent of the pre-estimated values. Aside from those previously described, three further free parameters are associated with each model: a scaling factor, S, a constant background contribution, b, and a term accounting for interface roughness in the samples, R .[8,23] The interfacial roughness parameter is distinct from the overall polydispersity in size of the objects. The polydispersity is mainly reflected on length-scales of the particle radius, i.e. at low q, while the roughness is a local lipid bilayer roughness of Gaussian nature that is visible in the very high-q end of the small-angle scattering data. Therefore our models are calculated following:

$$I(q) = S \cdot R \cdot n \cdot \langle P(q) \rangle_\Omega + b \tag{3}$$

where n is the particle number density of the sample and $\langle P(q) \rangle_\Omega$ is the form factor term including the usual $\Delta\rho^2 V^2$ terms and averaged over all possible orientations. The fraction of each molecule of α-synuclein inserted into the layer of lipid tails of the outer leaflet of the bilayer was fixed to 10% in line with the previously determined 14 residues .[24] 30% of

the protein is assumed to be in the Gaussian random coil formation to match the portion of the C-terminal thought to remain intrinsically disordered post-binding ,[13] which leaves 60% to be incorporated into the lipid headgroups of the outer leaflet. The dimensions of the protein proved to be difficult to determine with our modelling scheme and hence the radius of gyration,$R_{g\,\alpha\text{-syn}}$, of the C-terminal part that does not interact with the lipid bilayer, was fixed to 18Å throughout the study, as calculated by Kohn's power law relationship for 44 amino acids .[12] For the "Disc with Gaussian random coils" model w_{belt} was fixed to the diameter of an α-helix, 12Å.

Volumes and scattering lengths

Table S1: Chemical compositions, X-ray scattering lengths and neutron scattering lengths for the components required in the modelling.
∗Calculated using an average mass density of proteins 1.35 cm^2 g^{-1}.[16]
† .[20]
‡ .[14]

Component	Chemical composition	X-ray scattering length [cm]	Neutron scattering length [cm]	Estimated volume [Å^3]
Solvent	H_2O	$2.82 \cdot 10^{-12}$	-	30
Solvent	D_2O	-	$1.92 \cdot 10^{-12}$	30
α-synuclein	$C_{627}H_{1012}N_{166}O_{216}S_4$	$2.18 \cdot 10^{-9}$	-	17800*
PS headgroups	$C_8H_{11}NO_{10}PNa$	$4.85 \cdot 10^{-11}$	$8.82 \cdot 10^{-12}$	244†
DM tailgroups	$C_{26}H_{54}$	$5.92 \cdot 10^{-11}$	$-2.91 \cdot 10^{-12}$	734†
DMPS total	$C_{34}H_{65}NO_{10}PNa$	$2.08 \cdot 10^{-10}$	$5.91 \cdot 10^{-12}$	978†
DL tailgroups	$C_{22}H_{46}$	$5.02 \cdot 10^{-11}$	$-2.58 \cdot 10^{-12}$	619 ‡
DLPS total	$C_{30}H_{57}NO_{10}PNa$	$9.87 \cdot 10^{-11}$	$6.24 \cdot 10^{-12}$	912
d-α-synuclein	$C_{627}D_{782}H_{230}N_{166}O_{216}S_4$	-	$1.13 \cdot 10^{-9}$	17800*

Data processing

Pair-distance $(p(r))$ distributions were obtained by the Indirect Fourier Transform method using the online program *BayesApp* available at https://genapp.rocks.[25,26] SAXS data were re-binned to lie evenly on a log-scale.

Supplementary Results

Additional repeats and control experiments for the characterization of the α-synuclein interactions with DLPS and DMPS by SAXS

In this section, we provide some additional data of repeats and control experiments relevant for the stopped-flow SAXS experiments, as well as for the experiments designed to demonstrate the reversibility of the structural transitions that the lipid vesicles undergo upon interaction with α-synuclein. The figures in this section are referenced and discussed in the main manuscript and the experimental details are also provided there.
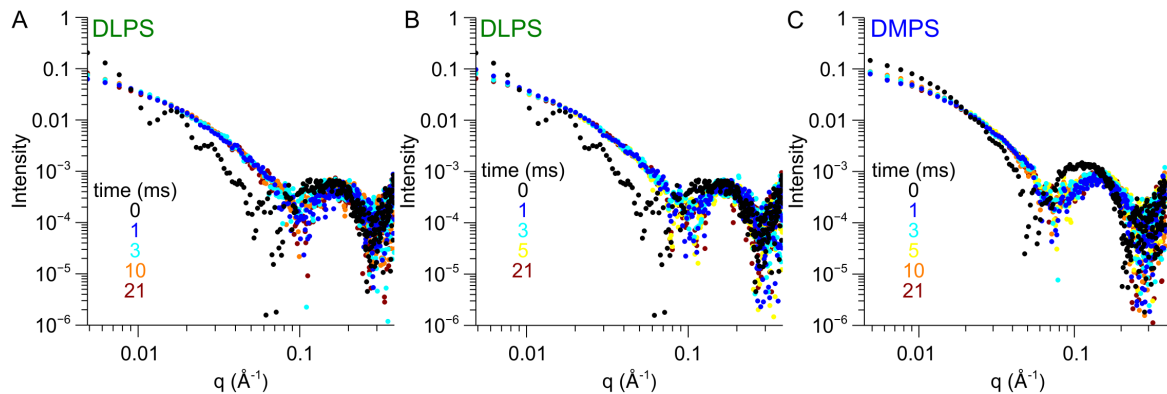

Figure S7: Additional repeats of the measurements shown in Figure 2 A-C. Change in the X-ray scattering function with time when 2 mM DLPS (A,B) or DMPS (C) was mixed with 70 μM α-synuclein using a stopped-flow set-up at 30°C.
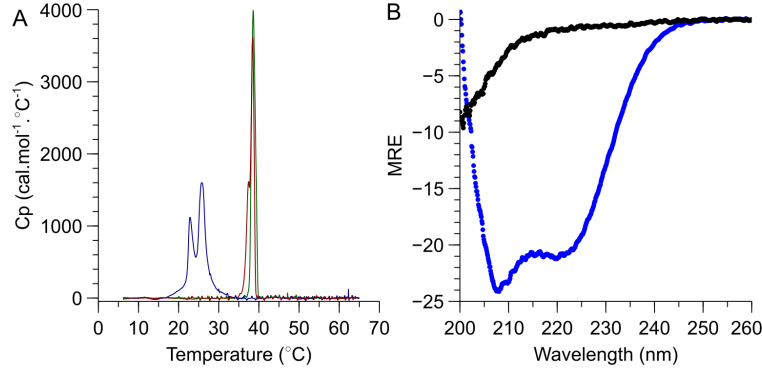
Figure S8: Differential scanning calorimetry and circular dichroism measurements of the α-synuclein:DMPS system before and after proteinase-K treatment. A. Differential scanning calorimetry scans of 0.86 mM DMPS in the absence (red) or the presence of 28.6 μM α-synuclein before (blue) and after (green) treatment with 1.7 μM PK for 1h at 20°C. B. Mean Residue Ellipticity spectrum of α-synuclein and DMPS measured at 37 °C before (blue) and after PK treatment (black). The samples were prepared by incubating 8 mM DMPS, 267 μM α-synuclein ± 15.7 μM PK for 1h and then diluted 10 times for the CD measurements.
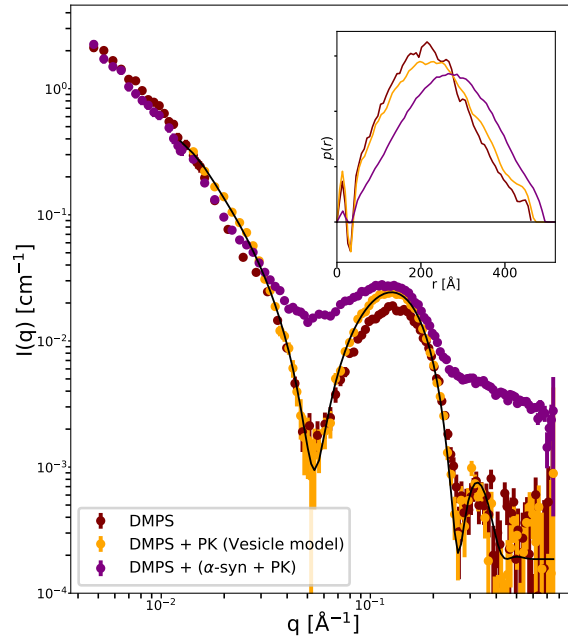

Figure S9: X-ray scattering control experiments for the PK-treatment of the DMPS:α-synuclein system. X-ray scattering profiles of 8 mM DMPS vesicles before (red) and after treatment with pK (orange), and in the presence of 270 μM α-synuclein pre-treated with pK (purple). The data were measured in phosphate buffer pH 6.5 at 37°C. The inserts show the p(r)-distribution profiles generated from the SAXS data.
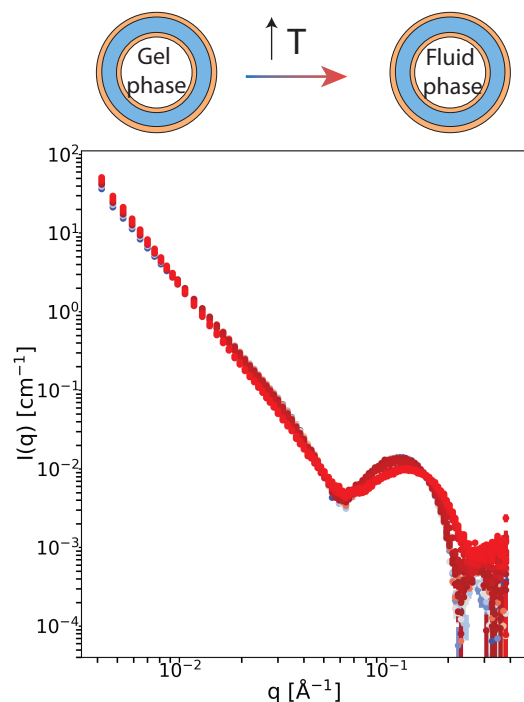
15

Figure S10: X-ray scattering profiles of DMPS model membranes at different temperatures. X-ray scattering profiles of 3 mM DMPS heated from 14 °C - 49 °C,
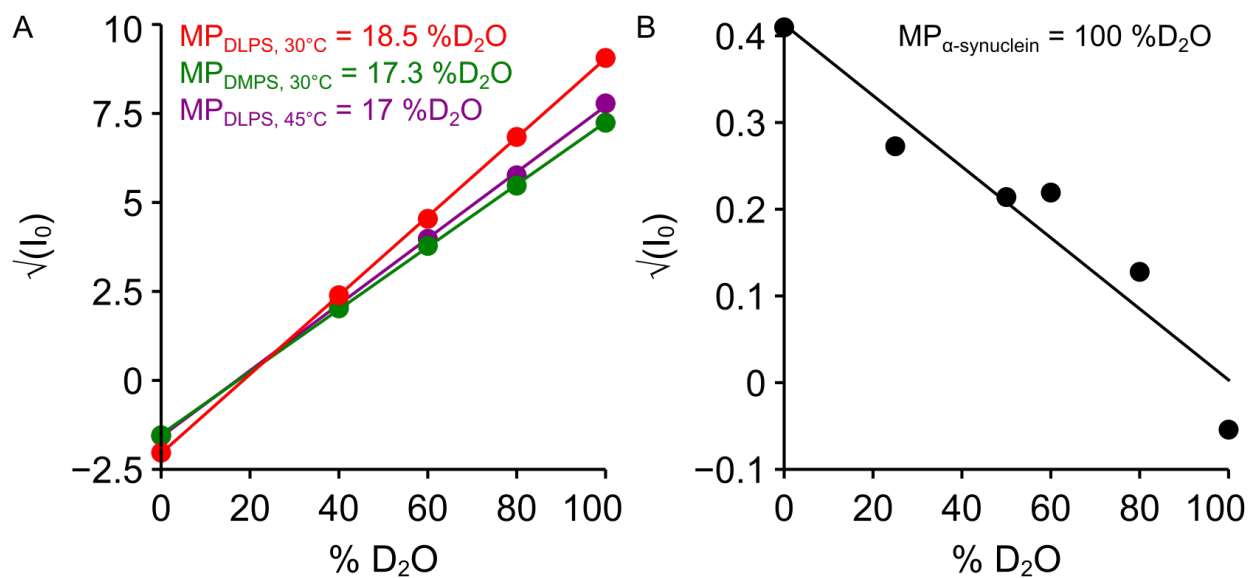

Figure S11: Determination of the contrast match points of the protein and DMPS and DLPS model membranes at different temperatures. A,B. Change in the square root of the intensity of the neutron scattering function of model membranes made with DLPS or DMPS (3mM) (A) or α-synuclein (200 μM) (B) at different temperatures. The samples were measured in 20 mM phosphate buffer pH 6.5.

Contrast-matching SANS measurements of the interactions between α-synuclein and DMPS and DLPS vesicles

Similar to the SAXS data presented in the main text, the SANS data clearly report a structural reorganisation of the initial lipid structures once α-synuclein is added. Under protein-matching conditions, i.e. 100% D_2O, we observed that the forward scattering intensity of the lipids decreased by more than an order of magnitude upon binding of the protein (Figure S12 A and B) which can be interpreted as a break down into particles of decreased volume. The low-q trends change from a slope of q^{-2}, indicative of planar structures such as vesicles or discs, to a gentler slope of q^{-1}, indicative of rod-like particles. The $p(r)$-distribution for pure DLPS (insets of Figure S12 A: purple) appears characteristic of well-formed liposomes ,[27] whereas for DMPS the $p(r)$-distribution appear to indicate polydisperse globular particles but the underlying structure is less clear. This mirrors our observations from our SAXS experiments (Figures 1, 2). The $p(r)$-distributions from the lipid:protein mixtures (Figure S12A and B insets: green) however, diverge from the SAXS since they are clearly characteristic of rod-like particles, featuring a sharp peak around $r = 50$ Å.

The polydisperse Three-shell vesicle model, described above, provides an excellent fit to the data from pure DLPS (Figure S12 A). The model fit requires a free scale parameter, increasing the theoretical scattering intensity by a factor 3, indicating there may be some errors with the concentration calculation. SANS is less sensitive to small changes in molecular volume and hence the volumes of the lipid headgroups, lipid tailgroups and α-synuclein are fixed at their pre-estimated values (Table S1) throughout the SANS analysis. We note, however, that akin to the SAXS modeling in Figure S10, we were unable to capture the full q-range of SANS data from pure DMPS as either vesicles or discs. We therefore again focus our modeling on the range $q = 0.01$ Å^{-1} and upwards, and the planar bilayer model to investigate properties of the bilayer rather than the whole structure. We speculate that the data contain a heterogeneous population of lipid aggregates but with a conserved bilayer structure. The results are presented in Table S2.
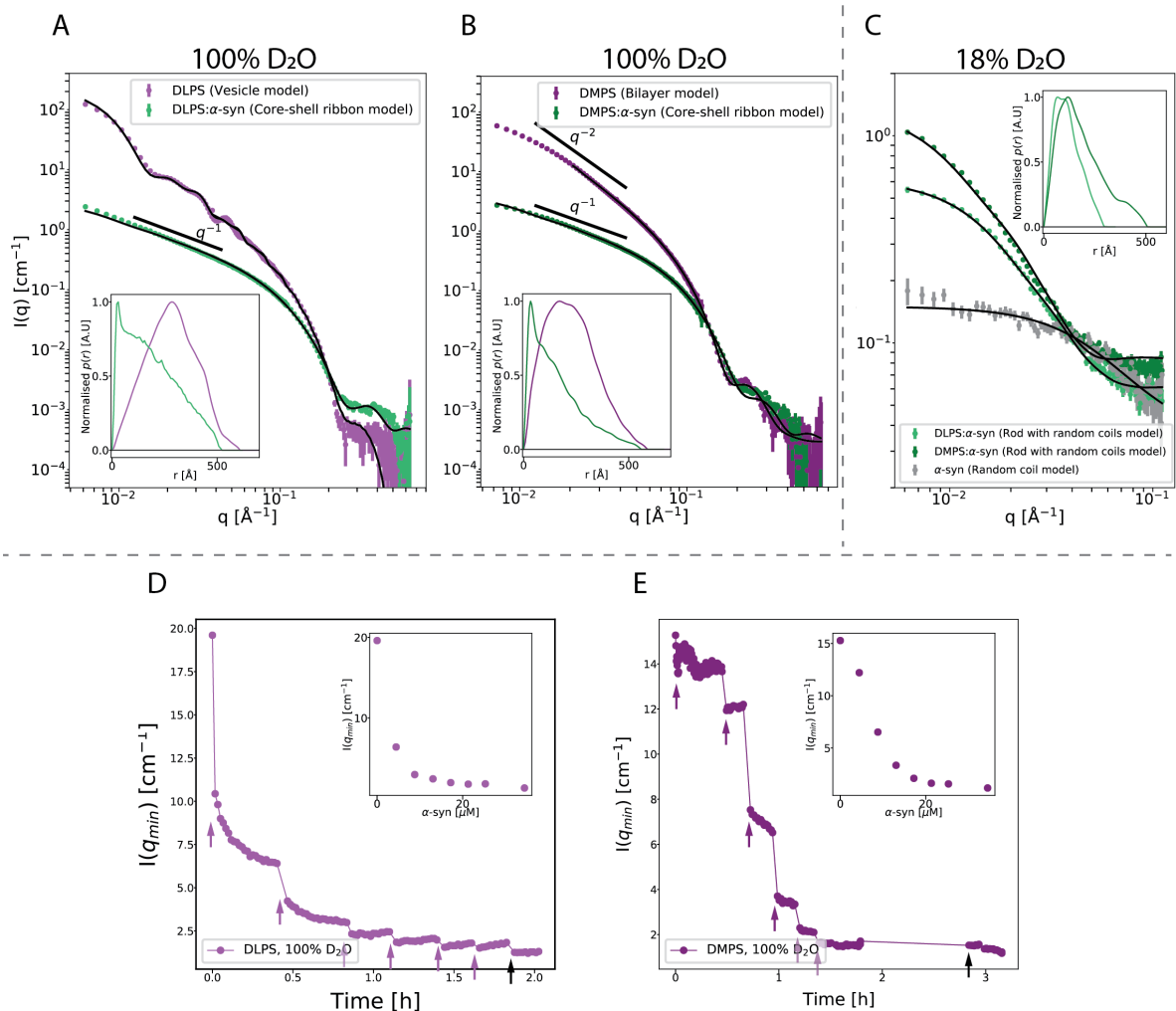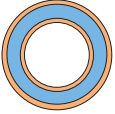
Figure S12: Structural characterisation of DMPS and DLPS model membranes upon binding of α-synuclein using SANS. (A,B) Neutron scattering function of 3 mM DLPS or DMPS meodel membranes (purples) and mixtures of model membranes and 100 μM deuterated α-synuclein (greens) measured at 30°C under protein contrast matching conditions, 100% D_2O. (C) Neutron scattering function of 100 μM α-synuclein (grey) and mixtures of DLPS or DMPS model membranes and α-synuclein (greens) measured under lipid matching conditions, 18% D_2O. The insets show the $p(r)$-distribution profiles generated from the SANS data. (D), (E). Change in the intensity at low q of the neutron scattering function (I_0), of DMPS (D) or DLPS (E) model membranes (1 mM lipid) measured under protein contrast matching conditions after addition of 4.4 μM (purple arrows) or 10 μM (black arrows) α-synuclein. Insets: Change in the fraction of protein bound to DMPS (D) or DLPS (E) model membranes with increasing α-synuclein calculated from change in SLD. The solution conditions in these experiments were phosphate buffer pH 6.5 and 30 °C.

We use a core-shell ribbon model to describe the lipid:α-synuclein co-structures as elongated particles with a rectangular cross-sectional area, as described in the section above. Since α-

synuclein is matched out under these experimental conditions we do not need to include the protruding Gaussian random coils in the model; however, the protein is implicitly included in calculations of the scattering length density of both shells. The model provides excellent fits to the data (Figure S12 A and B) and suggests the formation of rods with lengths between at least 500 and 650 Å and a distribution of widths. Although it is most probable that there is a distribution of sizes of particles, polydispersity in the length of the ribbon is not visible in our data. The ribbon model captures the local intensity maximum at $q = 0.2$ Å^{-1} well, suggesting it provides a good description of the bilayer structure which seems to remain present during the reorganisation of the lipids. The refined parameters imply slight asymmetry of the lipid structures, yielding 24 Å and 29 Å for the average cross-sectional width for DLPS and DMPS, respectively, compared to an average height of 39 Å for both types of lipids. We note that we also tried to fit this data with a cylindrical model which appears the same at low-q values but performed much worse at high-q.

Table S2: Left: Structural parameters refined from the SANS data in Figure S12 A (purple) using the Three-shell vesicle model. Right: Structural parameters refined from the SANS data in Figure S12 B (purple) using the Planar bilayer model. The fit was restricted to q > 0.015 Å^{-1} where intensity arising from bilayer features dominates. The models were calculated on absolute scale.

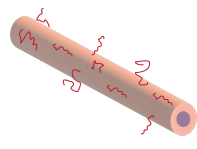| DLPS	Parameter	Values	DMPS	Parameter	Values
	Scale	3.37 ± 0.03		Scale	3.64 ± 0.05
	Radius [Å]	201 ± 19		t_{lipid} [Å]	20.4 ± 0.2
	σ_{Radius}	0.11 ± 0.001		σ_t	0.16 ± 0.03
	t_{lipid} [Å]	15.7 ± 0.1		Background [cm^{-1}]	0.00003 ± 0.0004
	σ_t	0.11 ± 0.03			
	Background [cm^{-1}]	0.00007 ± 0.0003			
	χ^2	211		χ^2	9.88

The neutron scattering data from deuterated α-synuclein (d-α-synuclein) alone in 18% D$_2$O can be well described with a simple Gaussian random coil model where the only free parameter is the radius of gyration (Figure S12 C). We refine an R_g of 30.6 ± 6.9 Å in good agreement with Kohn's estimation of 37 Å for 140 residues.[12] After addition of DMPS or DLPS model membranes to d-α-synuclein, we observed an increase in the scattering intensity at low-q values (q $\sim$ 0.06 Å^{-1}) suggesting that the apparent size of the protein particles

Table S3: Structural parameters refined from the SANS data in Figure S12 (green) using a core-shell ribbon model. *Parameters fixed during refinement.

Parameter	DLPS + d-α-synuclein	DMPS + d-α-syn
Scale	1.00*	1.00*
L/P	30*	30*
Shell thickness [Å]	2.37 ± 2.21	5.78 ± 3.02
Width [Å]	39.0 ± 4.7	39.2 ± 3.6
Height [Å]	24.4 ± 2.2	28.8 ± 2.7
Length [Å]	659 ± 160	539 ± 98
σ_{width}	0.33 ± 0.12	0.33 ± 1e-11
Background [cm^{-1}]	0.0002 ± 0.0004	0.0003 ± 0.0004
χ^2	22.7	8.84

Table S4: Structural parameters refined from the SANS data in Figure S12 C (green) using a core-shell rod with random coils model. *Parameters fixed during refinement.

Parameter	DLPS + d-α-synuclein	DMPS + d-α-synuclein
Scale	1.00*	1.00*
L/P	30*	30*
Shell thickness [Å]	4.67 ± 0.19	5.40 ± 0.17
Radius [Å]	26.7 ± 2.9	34.4 ± 2.1
Length [Å]	278 ± 74	465 ± 162
$R_{\text{g, }\alpha\text{-syn}}$	18*	18*
Background [cm^{-1}]	0.069 ± 0.007	0.092 ± 0.006
χ^2	1.71	5.70

increases upon binding to the lipids (Figure S12 C). The $p(r)$-distribution of the data from mixtures of DMPS and d-α-synuclein in 18% D$_2$O resemble large elongated structures but with a broader peak around r=150 Å as compared to the 100% D$_2$O data. This indicates a larger or less well-defined cross-section which could be explained by a corona of α-synuclein tails extending radially from the surface of the rod-like lipid particles. $p(r)$-distributions from DLPS:d-α-synuclein in 18% D$_2$O seem to represent shorter particles, also with a broader distribution of cross-sectional areas.

In order to model the lipid:d-α-synuclein structures contained in the 18% D$_2$O data, the contribution from the flexible part of protein must be taken into account. We built an analytical model representing a core-shell rod decorated with Gaussian random coils. The core and shell of the rods are assigned scattering length densities of lipid tailgroups and headgroups mixed with d-α-synuclein, respectively. In order to reduce the number of free parameters and avoid overfitting the model to these noisier data, we choose a monodisperse cylindrical rod rather than a ribbon. The differences in scattering profiles arising from cylindrical rods versus rectangular rods would be mostly indistinguishable within the limited q-range of the

data in Figure S12 C.

This model provides excellent fits to the data presented in Figure S12 C. The refined parameters are listed in Table S4. The refined values for the shell thickness and cylinder inner radius are in agreement with the dimensions refined from the data collected in 100% D_2O (Table S3). The average cylinder lengths, however, are shorter in comparison at 278 Åfor DLPS-d-α-synuclein. This could reflect some clustering or ordered arrangement of α-synuclein on the surface of the lipid particles.

In order to investigate the interaction in more detail, we performed a titration of the model membranes with d-α-synuclein under protein matching conditions, i.e. 100% D_2O (Figure S12 D,E), and we found that the decrease in forward scattering intensity was gradual with more added protein leading to a further decrease of the scattering intensity. Interestingly the observed decrease in signal intensity as a function of α-synuclein concentration was steeper than what would be predicted if the fraction of maximal binding was linearly related to the amount of bound protein (insets in Figure S12D and E). To understand this behaviour, we need to consider the cooperativity in protein binding to the membrane .[28] Two extreme scenarios can be envisioned: when protein molecules are introduced into an excess of lipids, they can either be distributed equally among the available lipid vesicles, or they can saturate some vesicles while leaving others unoccupied. The first scenario corresponds to the total absence of cooperativity, the second to full cooperativity. It has recently been reported that α-synuclein binding to lipids can be highly cooperative, under conditions where the vesicles remain largely intact .[28] The results of the titration experiments, in which we measured how the SANS scattering signal at low q-values decreased as a function of added protein, suggest however, that the interaction is less cooperative in our system. Given that the individual vesicles contribute independently to the scattering signal, their successive individual disruption under conditions of full cooperativity should lead to a linear decrease in signal intensity as a function of protein concentration. However, we observe a stronger than linear/proportional disruptive effect, suggesting that vesicles are only partly saturated, and

21

that partial saturation of a vesicle can lead to a higher than proportional loss in signal intensity. In other words, if a given vesicle is to 50% covered in protein, its scattering intensity will have dropped to below 50% of the initial value.

Different degrees of cooperativity in different α-synuclein lipid systems can be explained by the relative strength of the protein-lipid and protein-protein interactions, which may be shifted in the current study due to the use of different lipid systems and different buffer conditions.

Next, we investigated the structural change of the initial lipid structures due to α-synuclein binding by acquiring SANS data of the DMPS:α-synuclein mixtures at different temperatures ranging from 15 to 30 °C under both contrast-matching conditions (Figure S13 A, B). Under protein-matching conditions, i.e. 100% D_2O, we observed a decrease in the intensity at low q in the scattering profile of the mixture α-synuclein-DMPS with increasing temperature (Figure S13A). This transition was found to occur at a temperature of around 23 °C, a value matching that of the melting transition observed in the SAXS (Figure 3 A, inset) and DSC measurements [19] (Figure S8 A). Such a change in the SANS data was not observed for the pure DMPS model membranes with increasing temperatures (Figure S14 and inset to Figure S13 A), suggesting no structural re-arrangement of the lipids within the length scales corresponding to this range of q-values and similar to the observation by SAXS. Under lipid-matching conditions, i.e. 18% D_2O, we observed an increase in the intensity at low q of the scattering profile of the mixture α-synuclein-DMPS with increasing temperature, pointing towards an increase in the apparent size of the protein upon binding to the DMPS model membranes (Figure S13B). This transition also occurs at a temperature around 23 °C, the same value as that of the structural re-arrangement observed for the lipid model membranes (Figure S13B, inset). We once again interpret the decrease in forward scattering of the lipids upon protein binding as a break-up of the initial DMPS structures into smaller particles. We observe a transition of the slope from q^{-2} to q^{-1}, indicating the formation of rods as in the static SANS experiments above. The $p(r)$-distribution profiles also reflect a
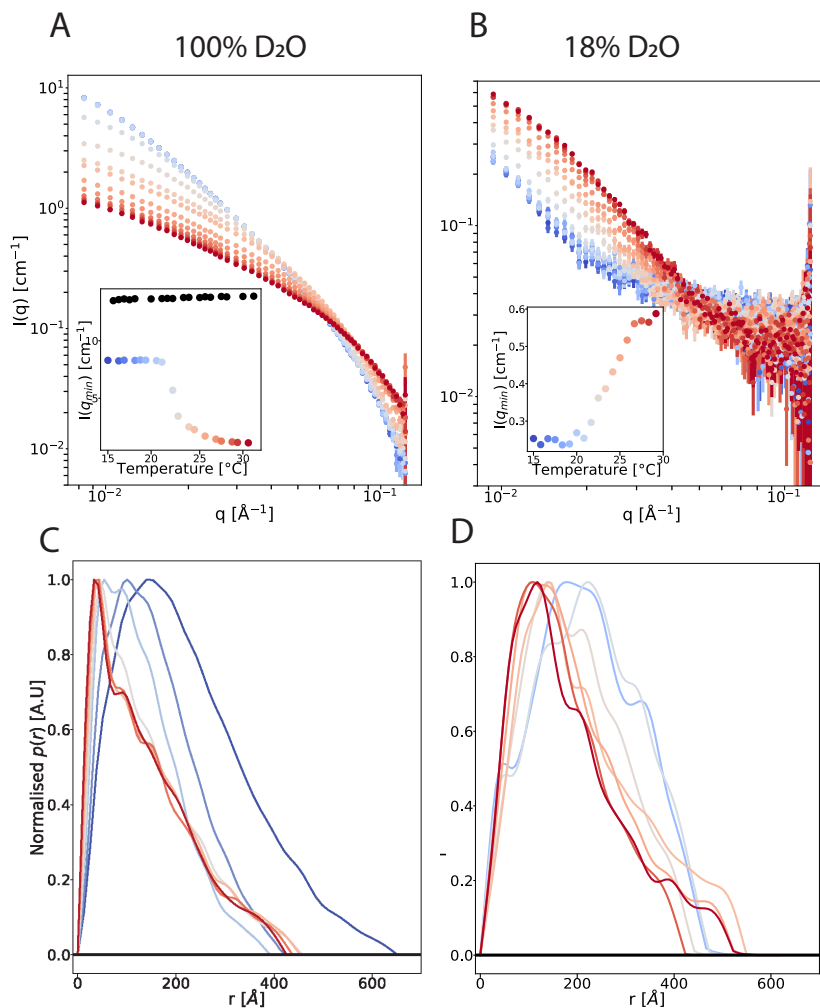
22

Figure S13: Structural characterisation of the α-synuclein:DMPS system at increasing temperature using SANS. Neutron scattering function of 3 mM DMPS and 100 μM α-synuclein measured under (A) protein matching conditions, 100% D_2O, or (B) lipid matching conditions, 18% D_2O. Insets: Change in scattering function at $q = 0.0073$ Å^{-1} as a function of temperature. Black: pure DMPS (SANS profiles not shown). (C) and (D) $p(r)$-distribution generated from the data demonstrating the system is undergoing structural changes.

transition from very large polydisperse objects at low temperatures to rod-like particles at higher temperatures ($> 25°$C).

We again attempted to refine form factors from this data series (Figure S15). Due to the more simple lipid contrast in SANS, as well as our limited q-range, we only considered simple geometrical volumes: either planes or cylinders. The particles here were assigned a "bulk" DMPS scattering length density. We find that the best description for the neutron scattering
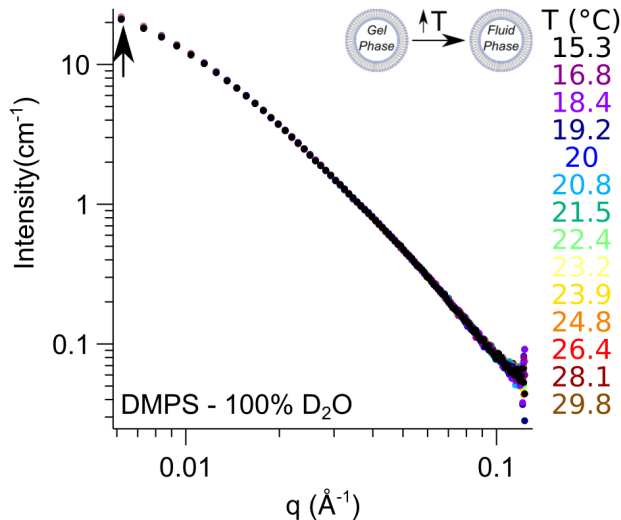
23

Figure S14: Neutron scattering function of DMPS model membranes (3 mM lipids) measured under protein (100% D_2O) contrast matching conditions with increasing temperature.

profile of the DMPS:α-synuclein system is as polydisperse planar structures, between 15 and 20 °C, or as rods between 26 and 30 °C with a length of ca. 430 Å and a radius decreasing from 26 to 22 Å (Figure S15 and Tables S5 and S6). We note that we can initially fit the model on absolute scale for the pure DMPS sample. Throughout the rest of the data series, however, the scale is a free fitting parameter. As the temperature is increased the refined scale decreases, reflecting some potential variation in SLD of the particle as d-α-synuclein binds to the lipids reducing the overall contrast or ambiguity in calculating the number density of scatterers.

Our analysis suggests that the observed transition of the vesicles to rod-like structures upon α-synuclein binding might pass through disc-like particles, specifically at 21 °C where cylinders of radius 130 Å and height 34 Å are refined from the data Figure S15). Around the transition temperature, around 23 °C, the data cannot be described adequately with either model, presumably due to the data containing a multi-modal distribution of structures.

The results of these temperature ramp experiments agree well with our initial SANS titration experiments (Figure S12 D,E), whereby protein and lipid were mixed at a temperature
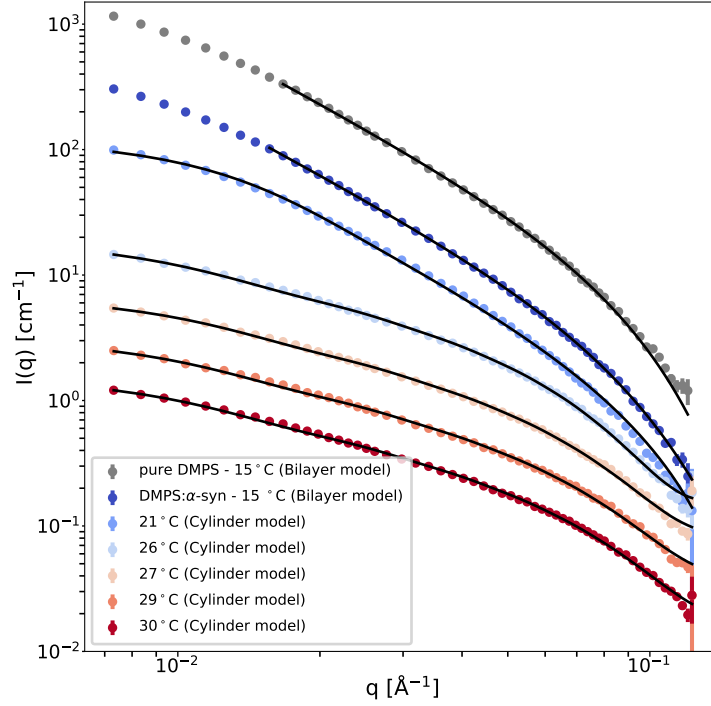
Figure S15: Structural modelling of the SANS data showing the evolution in the phospholipid particles with increasing temperature and hence binding of α-synuclein. For ease of viewing, the data are scaled by 2^n where n is the profile number, so the bottom scattering profile (red, 30°C) has n = 0 and remains on absolute scale, and the topmost profile (black) has n = 6. The refined structural parameters are listed in Tables S5 and S6.

Table S5: Structural parameters refined from the SANS data in Figure S15 using a simple planar model. *Parameter fixed during refinement.

	Parameter	DMPS, 15°C	DMPS + α-syn, 15°C
	Scale	1*	0.58 ± 0.04
	t_{lipid} [Å]	18.6 ± 0.3	17.3 ± 0.2
	σ_t	0.31 ± 0.07	0.30 ± 0.002
	χ^2	3.81	1.77

Table S6: Structural parameters refined from the SANS data in Figure S15 using a simple cylinder model model. - means the parameter was not required to during refinement from that data set.

	Parameter	21°C	26°C	27°C	29 °C	30 °C
	Scale	0.59 ± 0.06	0.43 ± 0.01	0.42 ± 0.01	0.42 ± 0.01	0.42 ± 0.01
	Radius [Å]	134 ± 2	25.7 ± 0.3	22.9 ± 0.3	21.6 ± 0.4	21.4 ± 0.4
	σ_{Radius}	0.33 ± 0.04	-	-	-	-
	Length [Å]	34.4 ± 3.85	451 ± 49	421 ± 45	431 ± 51	432 ± 52
	χ^2	23.9	20.8	14.2	11.3	8.5

where the binding immediately induces melting of the lipid. In both scenarios the addition of the protein to the outer layer of the bilayer induces a decrease in protein-matched lipid SANS intensity at low q values and an increase in lipid-matched protein SANS intensity at low q values. Our modeling of the corresponding SAXS data shows that the interaction between α-synuclein and DMPS planar bilayer structures leads to a break-up of the lipid structures into significantly smaller particles that are best modelled as discs. The SANS data are in qualitative agreement with this conclusion, and show a decrease of the size of the protein-matched planar bilayer structures and an increase of the apparent size of α-synuclein from that of a single protein molecule towards that of a larger lipid-protein particle. However, in the case of the SANS data, the modelling suggests that the particles are best described as short, thin rods. This discrepancy between these models will be discussed below.

The reversible break up of DMPS and DLPS vesicles into small particles upon α-synuclein binding is confirmed by dynamic light scattering measurements

We also performed DLS experiments in microcapillaries and we subjected different mixtures of α-synuclein and extruded DLPS/DMPS lipids to thermal scanning at two different rates (0.5 and 5°C/min) from 15 to 35°C, and back. Figure S16 shows representative data for 1 mM DLPS in the presence of 95 μM (excess) and 9.5 μM (sub-stoichiometric) α-synuclein, acquired at scan rates of 0.5 °C/min and 5 °C/min. Similarly, Figure S17 shows representative data for 1 mM DMPS in the presence of 95 μM (excess) and 9.5 μM (sub-stoichiometric) α-synuclein, acquired at scan rates of 0.5 °C/min and 5 °C/min. The results of these DLS experiments, in which also the absolute light scattering intensity was measured, can be summarised as follows. The addition of α-synuclein to DLPS vesicles leads to a decrease in size and scattering intensity at both protein concentrations, with the strongest effect at the highest concentration. Only at the higher concentration, a clear evolution with increasing

temperature is observed, whereby the particles appear to become gradually smaller. This process is not reversible upon cooling back down to 15°C, because even at this lower temperature limit attainable in this experiment, the lipid is in the fluid phase if protein is bound. In the case of DMPS, the particles in the protein-lipid mixture at temperatures below the melting temperature are bigger than pure lipids (reflecting the size of the vesicles with a protein corona), but upon heating both the size and scattering intensity decrease significantly and sharply. It is worth noting here that the size range meaured by DLS for the DMPS is very similar to that of DLPS and hence indicative that vesicles form a significant fraction of the structures. However, together with the SAXS and SANS data, a picture of more complex composition, comprising both vesicles and large bilayer structures, emerges for DMPS. The transition into smaller structures observed for DMPS upon heating is in large parts reversible (more so at the lower protein concentration), but displays significant hysteresis. The change in size and scattering intensity induced by protein binding is more pronounced for DLPS compared to DMPS. In the case of DMPS, a clear scan rate dependence can be observed, but only during the cooling step. This is consistent with stopped-flow SAXS data that showed that the initial binding step is approximately diffusion limited. The detachment of protein induced by cooling down, on the other hand, appears to be significantly slower and a clear difference can be seen between 0.5 °C/min and 5 °C/min. The overall conclusions from the DLS experiments are thus in excellent agreement with, and provides a model-free confirmation of, the results obtained from the modeling of our SAXS and SANS data. The finding that in the case of DMPS a protein concentration (9.5 μM) three-fold below the nominal saturation concentration leads to an effect on particle size and scattering intensity of very similar magnitude compared to a concentration ca. 3-fold above the saturation concentration (95 μM) provides additional evidence for the low degree of cooperativity of the system. If the binding were highly cooperative, in the case of 9.5 μM, only about 1/3 of the vesicles should be disrupted and hence one would at most expect a drop in scattering intensity by 1/3. However, the observed decrease is of the order of 4-5, suggesting that most, if not

all, vesicles are significantly disrupted and that is only possible if the protein is distributed approximately equally over all vesicles, in turn suggesting a low degree of cooperativity.
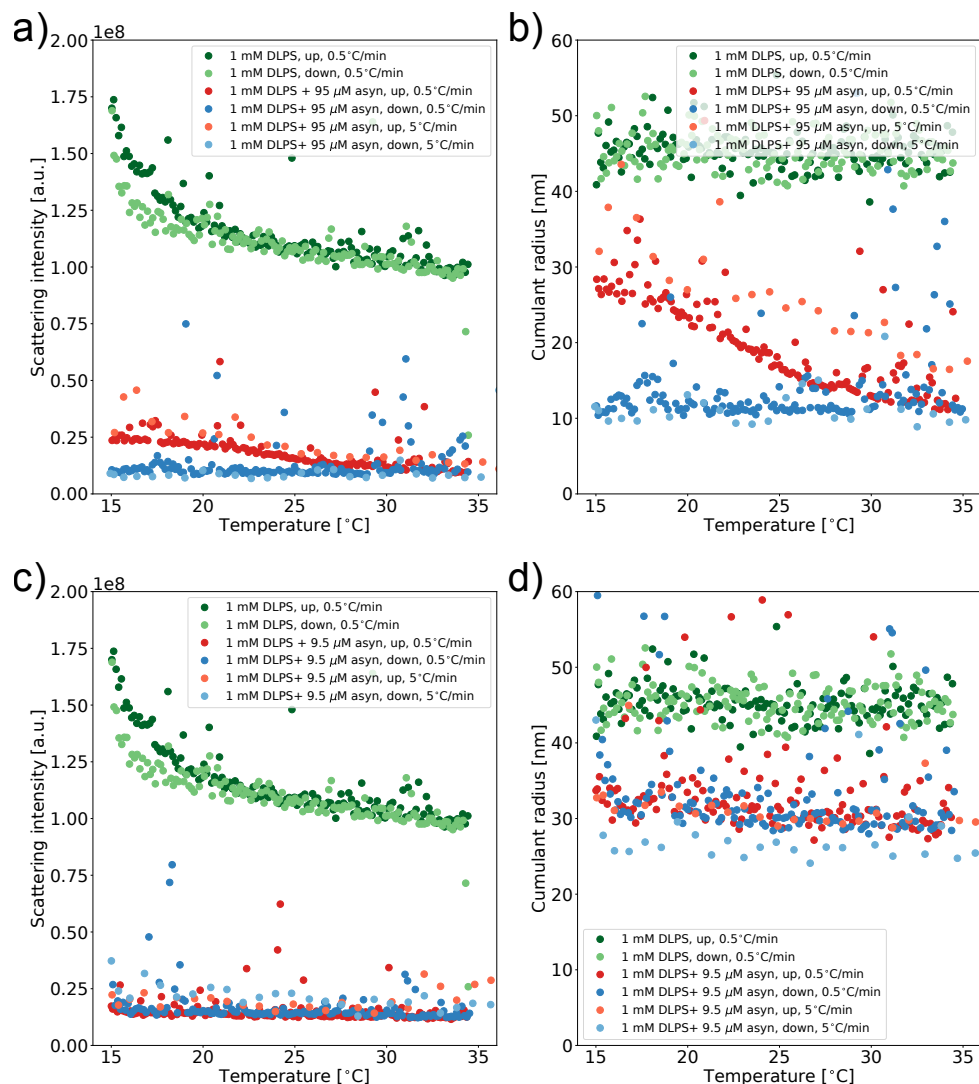

Figure S16: Temperature-dependent DLS experiments of DLPS vesicles in the absence or presence of different concentrations of α-synuclein. DLPS (1 mM) vesicles were incubated in the absence (green) or the presence of 95 μM (a,b) or 9.5 μM (c,d) α-synuclein at increasing (dark colours) or decreasing (light colours) temperature and scan rates of 0.5°C / min and 5°C / min. The scattering intensity (a,c) and cumulant radius (b,d) are shown.
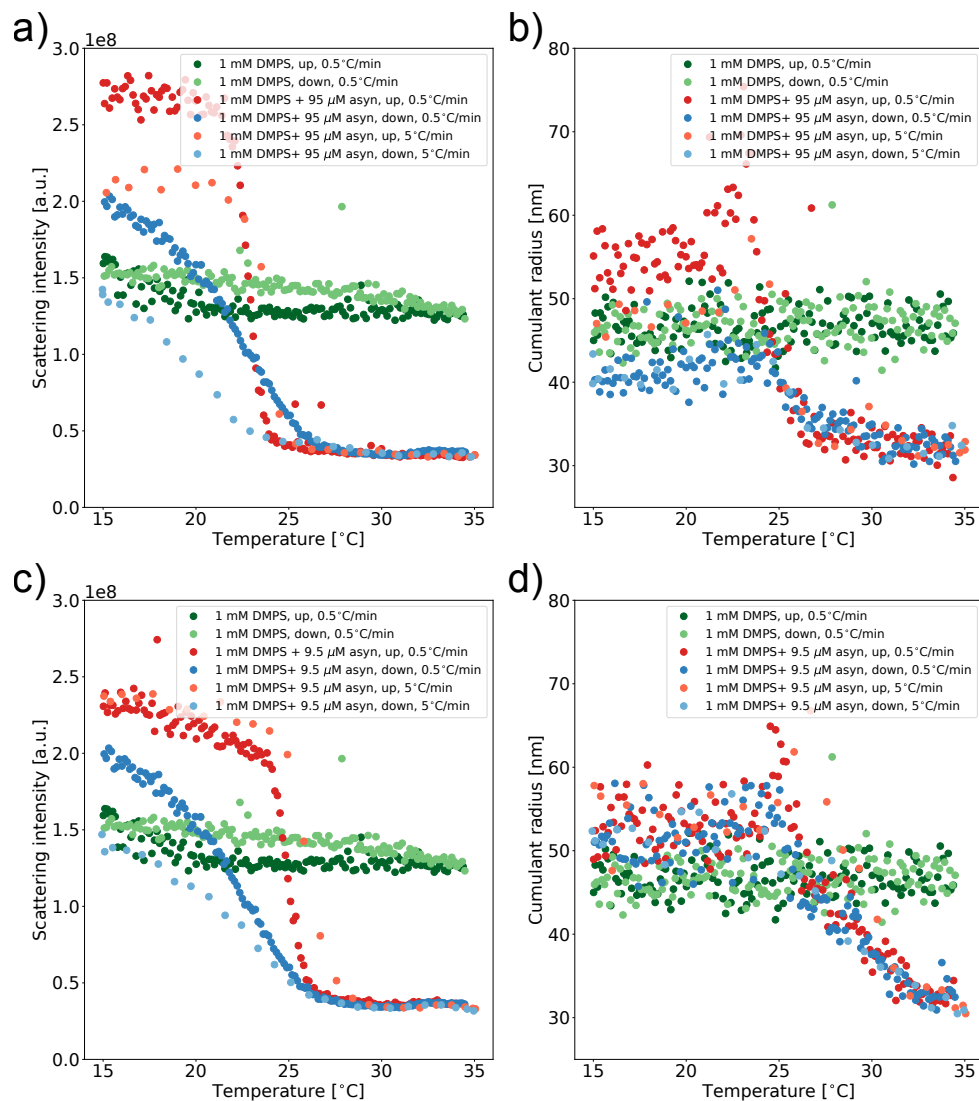
Figure S17: Temperature-dependent DLS experiments of DMPS vesicles in the absence or presence of different concentrations of α-synuclein. DMPS (1 mM) vesicles were incubated in the absence (green) or the presence of 95 μM (a,b) or 9.5 μM (c,d) α-synuclein at increasing (dark colours) or decreasing (light colours) temperature and scan rates of 0.5°C/min and 5°C/min. The scattering intensity (a,c) and cumulant radius (b,d) are shown.

References

(1) Nallet, F.; Laversanne, R.; Roux, D. Modelling X-ray or neutron scattering spectra of lyotropic lamellar phases: interplay between form and structure factors. *Journal de Physique II* **1993**, *3*, 487–502.

(2) Berghausen, J.; Zipfel, J.; Lindner, P.; Richtering, W. Influence of water-soluble polymers on the shear-induced structure formation in lyotropic lamellar phases. *The Journal of Physical Chemistry B* **2001**, *105*, 11081–11088.

(3) Debye, P. Molecular-weight determination by light scattering. *The Journal of Physical Chemistry* **1947**, *51*, 18–32.

(4) Skar-Gislinge, N.; Simonsen, J. B.; Mortensen, K.; Feidenhans'l, R.; Sligar, S. G.; Lindberg Møller, B.; Bjørnholm, T.; Arleth, L. Elliptical structure of phospholipid bilayer nanodiscs encapsulated by scaffold proteins: Casting the roles of the lipids and the protein. *Journal of the American Chemical Society* **2010**, *132*, 13713–13722.

(5) Skar-Gislinge, N.; Arleth, L. Small-angle scattering from phospholipid nanodiscs: Derivation and refinement of a molecular constrained analytical model form factor. *Physical Chemistry Chemical Physics* **2011**, *13*, 3161–3170.

(6) Cholak, E.; Bucciarelli, S.; Bugge, K.; Vestergaard, N. T. J. B.; Arleth, L.; Kragelund, B. B.; Langkilde, A. E. Distinct α-Synuclein:Lipid Co-Structure Complexes Affect Amyloid Nucleation Through Fibril Mimetic Behavior. *Biochemistry* **2019**, *58*, 5052–5065.

(7) Pedersen, J. S.; Gerstenberg, M. C. Scattering form factor of block copolymer micelles. *Macromolecules* **1996**, *29*, 1363–1365.

(8) Pedersen, J. S. Form factors of block copolymer micelles with spherical, ellipsoidal and cylindrical cores. *Journal of Applied Crystallography* **2000**, *33*, 637–640.

(9) Arleth, L.; Ashok, B.; Onyuksel, H.; Thiyagarajan, P.; Jacob, J.; Hjelm, R. P. Detailed structure of hairy mixed micelles formed by phosphatidylcholine and PEGylated phospholipids in aqueous media. *Langmuir* **2005**, *21*, 3279–3290.

(10) Eichmann, C.; Campioni, S.; Kowal, J.; Maslennikov, I.; Gerez, J.; Liu, X.; Verasdonck, J.; Nespovitaya, N.; Choe, S.; Meier, B. H.; Picotti, P.; Rizo, J.; Stahlberg, H.; Riek, R. Preparation and Characterization of Stable alpha-Synuclein Lipoprotein Particles. *J Biol Chem* **2016**, *291*, 8516–8527.

(11) Viennet, T.; Wördehoff, M. M.; Uluca, B.; Poojari, C.; Shaykhalishahi, H.; Willbold, D.; Strodel, B.; Heise, H.; Buell, A. K.; Hoyer, W.; Etzkorn, M. Structural insights from lipid-bilayer nanodiscs link α-Synuclein membrane-binding modes to amyloid fibril formation. *Communications biology* **2018**, *1*, 44.

(12) Kohn, J. E.; Millett, I. S.; Jacob, J.; Zagrovic, B.; Dillon, T. M.; Cingel, N.; Dothager, R. S.; Seifert, S.; Thiyagarajan, P.; Sosnick, T. R., et al. Random-coil behavior and the dimensions of chemically unfolded proteins. *Proceedings of the National Academy of Sciences* **2004**, *101*, 12491–12496.

(13) Fusco, G.; Simone, A. D.; Gopinath, T.; Vostrikov, V.; Vendruscolo, M.; Dobson, C. M.; Veglia, G. Direct observation of the three regions in α-synuclein that determine its membrane-bound behaviour. *Nat Commun* **2014**, *5*, 3827.

(14) Armen, R. S.; Uitto, O. D.; Feller, S. E. Phospholipid component volumes: Determination and application to bilayer structure calculations. *Biophys. J.* **1998**, *75*, 734–744.

(15) Szekely, P.; Dvir, T.; Asor, R.; Resh, R.; Steiner, A.; Szekely, O.; Ginsburg, A.; Mosenkis, J.; Guralnick, V.; Dan, Y.; Wolf, T.; Tamburu, C.; Raviv, U. Effect of Temperature on the Structure of Charged Membranes. *The Journal of Physical Chemistry B* **2011**, *115*, 14501–14506.

(16) Mylonas, E.; Svergun, D. I. Accuracy of molecular mass determination of proteins in solution by small-angle X-ray scattering. *Journal of applied crystallography* **2007**, *40*, s245–s249.

(17) Glatter, O. A new method for the evaluation of small-angle scattering data. *J. Appl. Crystallogr.* **1977**, *10*, 415–421.

(18) Johansen, N. T.; Luchini, A.; Tidemand, F. G.; Orioli, S.; Martel, A.; Porcar, L.; Arleth, L.; Pedersen, M. C. Structural and Biophysical Properties of Supercharged and Circularized Nanodiscs. *Langmuir* **2021**, *37*, 6681–6690.

(19) Galvagnion, C.; Brown, J. W. P.; Ouberai, M. M.; Flagmeier, P.; Vendruscolo, M.; Buell, A. K.; Sparr, E.; Dobson, C. M. Chemical properties of lipids strongly affect the kinetics of the membrane-induced aggregation of α-synuclein. *Proceedings of the National Academy of Sciences of the United States of America* **2016**, *113*, 7065–7070.

(20) Petrache, H. I.; Tristram-Nagle, S.; Gawrisch, K.; Harries, D.; Parsegian, V. A.; Nagle, J. F. Structure and Fluctuations of Charged Phosphatidylserine Bilayers in the Absence of Salt. *Biophysical Journal* **2004**, *86*, 1574–1586.

(21) Pedersen, J. S. Analysis of small-angle scattering data from colloids and polymer solutions: Modeling and least-squares fitting. *Adv. Colloid Interface Sci.* **1997**, *70*, 171–210.

(22) Pedersen, M. C.; Arleth, L.; Mortensen, K. WillItFit: a framework for fitting of constrained models to small-angle scattering data. *Journal of Applied Crystallography* **2013**, *46*, 1894–1898.

(23) Als-Nielsen, J.; McMorrow, D. *Elements of Modern X-ray Physics: Second Edition*; John Wiley and Sons, 2011.

(24) Cholak, E.; Bugge, K.; Khondker, A.; Gauger, K.; Pedraz-Cuesta, E.; Pedersen, M. E.; Bucciarelli, S.; Vestergaard, B.; Pedersen, S. F.; Rheinstädter, M. C.; Langkilde, A. E.; Kragelund, B. B. Avidity within the N-terminal anchor drives α-synuclein membrane interaction and insertion. *FASEB Journal* **2020**, *34*, 7462–7482.

(25) Hansen, S. Bayesian estimation of hyperparameters for indirect Fourier transformation in small-angle scattering. *Journal of Applied Crystallography* **2000**, *33*, 1415–1421.

(26) Savelyev, A.; Brookes, E. GenApp: Extensible tool for rapid generation of web and native GUI applications. *Future Generation Computer Systems* **2019**, *94*, 929–936.

(27) Glatter, O. In *Scatt. Methods their Appl. Colloid Interface Sci.*; Glatter, O., Ed.; Elsevier, 2018; pp 33–74.

(28) Makasewicz, K.; Wennmalm, S.; Stenqvist, B.; Fornasier, M.; Andersson, A.; Jonsson, P.; Linse, S.; Sparr, E. Cooperativity of α-Synuclein Binding to Lipid Membranes. *ACS Chemical Neuroscience* **2021**, *12*, 2099–2109.